ISSA-BASED NOISE REDUCTION AND CONTROL OPTIMIZATION FOR ENERGY STORAGE CONVERTERS IN THE POWER IoT

Yuanliang FAN, Zewen LI*, Weiming CHEN, Jianli LIN, Xinghua HUANG, Lingfei LI[1]

Currently, energy storage converters in the power Internet of Things face challenges caused by the coupling between high-frequency switching and dynamic control. In order to address this issue, a novel energy storage inverter noise reduction and control optimization model combining improved sparrow search algorithm and multi-objective particle swarm optimization algorithm was proposed, which integrates the Improved Sparrow Search Algorithm and the Multi-Objective Particle Swarm Optimization Algorithm. The model enhances the search ability for noise spectrum features by introducing adaptive inertia weights. Experimental results show that this model achieves the most effective noise suppression, with a total harmonic distortion of 1.32%, which is significantly lower than those of the comparison models. The total harmonic distortions of the optimal order adaptive model combining the Improved Sparrow Search Algorithm and the Dung Beetle Optimizer with Variational Mode Decomposition reach 2.64% and 3.25%, respectively. The Continuous Wavelet Transform combined with the Least Mean Square method shows the highest voltage fluctuation at ±2.17%, while the proposed model limits it to only ±0.31%. The noise generated by this model also presents a distribution pattern that is closest to the actual recorded noise in terms of amplitude. In contrast, the comparison models show significant differences in normalized frequency within the -0.05-0.05 mV range, indicating lower simulation accuracy. These results demonstrate the proposed model's excellent noise suppression and operational efficiency, offering a practical solution for the coordinated optimization of noise and energy efficiency in power Internet of Things equipment. At the same time, breaking through the limitations of traditional single algorithms, an innovative population initialization strategy based on elite reverse learning has been designed.

Keywords: Power internet of things; Improved sparrow search algorithm; Energy storage converter; Multi-objective particle swarm optimization; Noise reduction

1. Introduction

With the strong promotion of the "dual carbon" goal, the installed capacity of energy storage converters in the power Internet of Things (IoT) continues to grow

[1] State Grid Fujian Electric Power Research Institute, Fuzhou, China
*Corresponding author, E-mail: zewenlizw@outlook.com

at an increasing annual rate. However, high-frequency switching noise has become a major obstacle to large-scale equipment deployment, as high-density setups often cause noise pollution [1–2]. From a control coupling perspective, there is a parameter conflict between the Proportional-Integral-Derivative controller and noise suppression strategies [3]. Existing noise reduction methods suffer from high modal aliasing rates and premature convergence under dynamic load conditions, which do not meet the modular deployment requirements of power IoT equipment [4]. Traditional algorithms may achieve noise reduction in specific frequency bands when dealing with high-dimensional nonlinear problems, but they fail to fully consider the system's dynamic control response [5]. Current research often treats noise reduction and control as separate objectives, which easily leads to reduced overall system efficiency. The Improved Sparrow Search Algorithm (ISSA) features strong adaptability and uses cubic mapping to initialize the population, solving the problem of uneven distribution caused by traditional random initialization. The Multi-Objective Particle Swarm Optimization Algorithm (MOPSO) is effective in handling multiple objectives simultaneously, allowing it to identify several Pareto optimal solution sets. To better achieve both noise reduction and control for energy storage converters, this paper proposes a control optimization model based on a combination of MOPSO and ISSA (MOPSO-ISSA). The model constructs a multi-objective optimization function to search for Pareto optimal solutions. The novelty of this work lies in integrating the global search ability of MOPSO with the local refinement ability of the improved ISSA, forming a multi-objective coupling model. This model aims to solve the technical challenges of coordinated optimization involving multiple objectives in energy storage converters.

2. Related works

ISSA, as a novel swarm intelligence optimization method, aimed to solve the problems of local optimum trapping and slow convergence in the original algorithm by integrating various strategies. Some researchers explored its characteristics. Gharehchopogh F S et al. introduced the Sparrow Search Algorithm to address the limitations of traditional optimization methods. Their experimental results showed that the algorithm performed well in terms of improvement, mutation, and optimization. Compared to mathematical programming, it offered advantages such as fewer parameters and strong resistance to local optima [6]. Xue J et al. studied the search mechanism and implementation process of the Sparrow Search Algorithm to overcome the tendency of traditional algorithms to fall into local optima. Their findings indicated that the algorithm improved global search ability and convergence speed by simulating the foraging and anti-predation behaviors of sparrows [7]. Cen J et al. proposed a coordinated optimization method based on ISSA to reduce energy consumption in central air-conditioning systems.

Simulation experiments confirmed that the method effectively lowered energy usage and showed fast convergence [8]. MOPSO has been widely used to solve multi-objective optimization problems. This method determined particle flight directions through Pareto dominance and maintained a global repository of previously identified non-dominated vectors. Several researchers contributed different views on its application. Zhang W et al. proposed a hybrid algorithm based on MOPSO to address energy consumption issues in distributed flow shop scheduling. Experiments revealed that their method shortened completion time and reduced energy usage by learning and optimizing particle swarm search strategies [9]. Shu X et al. developed a hybrid algorithm based on MOPSO to address the lack of diversity in multi-objective optimization algorithms. According to their results, the proposed method effectively adjusted population size through archive resources and significantly improved the coverage of the Pareto front [10].

In addition, noise reduction and control optimization of energy storage converters are key to improving the overall performance of energy storage systems. Noise reduction relies on source control, intelligent adjustment, and transmission blocking, while control optimization depends on advanced algorithms and topological upgrades to improve both efficiency and noise control. Many researchers have studied this topic. Cao Y et al. proposed a hybrid algorithm to reduce winding loss while addressing the common-mode noise and control challenges in bidirectional converters. A series of experiments showed that this method effectively reduced noise and enabled real-time closed-loop control [11]. Nabih A and Li Q developed a resonant matrix inductor integrated topology to address power efficiency and cost issues in data centers. Their experiments demonstrated improved peak efficiency and reduced common-mode noise [12]. Babayomi O et al. introduced a parallel cascaded extended state observer to tackle issues of disturbance rejection and noise suppression in model predictive control. Their results showed outstanding performance in both aspects [13]. Vaithianathan M proposed a novel approach that combined digital signal processing algorithms to suppress noise in speech signals. Simulation experiments confirmed that this method improved signal-to-noise ratio and reduced word error rate [14]. Yu Z et al. aimed to improve the energy efficiency of analog-to-digital converters by designing a time-domain second-order noise shaping architecture. Their results showed significantly reduced power consumption and effective adaptation to different oversampling ratio requirements [15].

According to findings from both domestic and international researchers, current noise reduction technologies have made considerable progress. However, problems still exist, including the high cost of multilevel topologies and insufficient real-time performance and robustness. Model predictive control requires high-precision system models, but in practical scenarios, the time-varying characteristics of battery parameters often lead to increased delays in dynamic response. To further

optimize noise reduction and control of converters, this study integrates MOPSO and ISSA to construct a control optimization model for energy storage converters. The goal is to adapt the model to voltage prediction scenarios in power IoT energy storage converters and provide a reliable foundation for future noise reduction and control optimization.

2. Construction of the MOPSO-ISSA-based noise reduction and control optimization model for energy storage converters

2.1 Design of the ISSA-based noise reduction strategy for energy storage converters

ISSA improves global search capability by introducing multiple strategies. It adaptively adjusts coefficients and uses a dynamic sine disturbance strategy to quickly converge to the optimal solution. Therefore, this study uses ISSA to design a noise reduction strategy for energy storage converters in power systems, aiming to better meet the high-precision control requirements and optimize key parameters in the noise reduction process. The core improvement mechanism of ISSA is shown in Fig. 1.

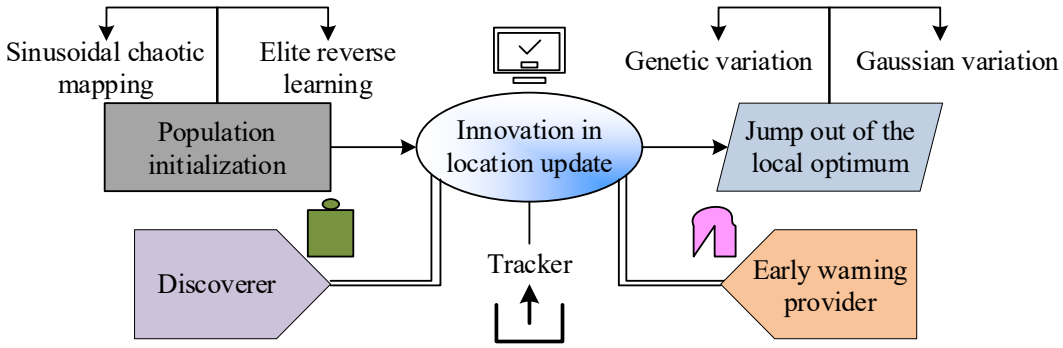

Fig. 1 Schematic diagram of the core improvement mechanism of ISSA (Source from: author self-drawn)

In Fig. 1, population initialization is optimized using sine chaotic mapping to generate the initial population. The elite opposition-based learning mechanism expands the search coverage by generating an opposite solution from the current best solution. The position update strategy includes three phases: discoverer, follower, and warner. In the discoverer phase, the Lévy flight strategy is integrated. The follower phase introduces a dynamic sine disturbance factor, and the warner phase adopts a Gaussian shift strategy to enhance local exploitation accuracy. The position update equation for followers is shown in Equation (1)[16].

$$X_{i,j}^{t+1} = Q \cdot \exp(\frac{X_{worst}^{t} - X_{i,j}^{t}}{i^2}) \quad (\text{i} > \text{n}/2) \tag{1}$$

In Equation (1), where $X_{i,j}^{t}$ represents the position of the i-th follower in the j-th dimension during the t-th iteration. X_{worst}^{t} is the position of the worst individual in the current population. Q is a random number that follows a standard normal distribution. n represents the total population size, and $\exp(\cdot)$ is the exponential function. The position update equation for warners is shown in Equation (2) [17].

$$J = X_{best}^{t} + \beta \cdot \left| X_{i,j}^{t} - X_{best}^{t} \right| \tag{2}$$

In Equation (2), where β denotes the step size control parameter, X_{best}^{t} denotes the position of the individual with the best fitness in the current population. Finally, the embedded mutation operation based on genetic operators randomly perturbs some individual positions, increasing the population diversity. Key technologies for noise control of energy storage converters require coordinated optimization across multiple aspects such as source suppression and propagation blocking. These core technologies are illustrated in Fig. 2.

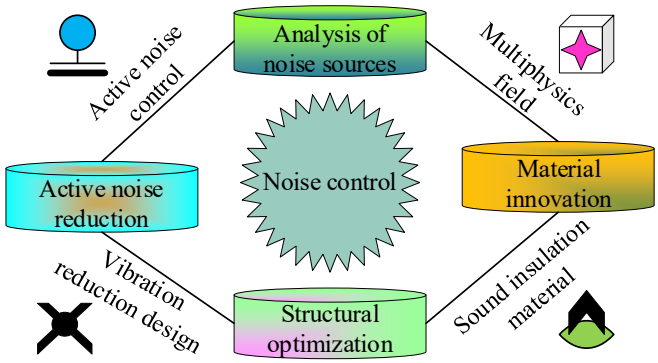

Fig. 2 Schematic diagram of key technologies for noise control in energy storage converters (Source from: author self-drawn)

As shown in Fig. 2, the noise of energy storage converters comes from various sources, including motor drive systems, inverter high-frequency switching, and cooling devices. The main noise sources can be located using multi-physics field coupling analysis. Advanced sound insulation materials suppress vibration transmission and reduce resonance noise of equipment. The cutoff frequency of the low-pass filter is calculated using Equation (3).

$$f_C = \frac{1}{2\pi\sqrt{LC}} \tag{3}$$

In Equation (3), where L and C represent the inductance and capacitance

values, respectively. The virtual impedance regulation is calculated using Equation (4).

$$Z_v = R_v + ywL_v \tag{4}$$

In Equation (4), where R_v and L_v are the virtual resistance and virtual inductance, respectively. w is the angular frequency, and y denotes the imaginary unit. Structural optimization and active noise reduction involve vibration isolation design and active noise control. Buffer pads are added between battery modules to optimize the inverter cooling structure. Meanwhile, sound wave interference technology is applied to generate real-time inverse sound waves that cancel the noise, which is especially effective in suppressing high-frequency switching noise of converters. Subsequently, this study designs a noise reduction strategy for power system energy storage converters based on ISSA, as shown in Fig. 3.

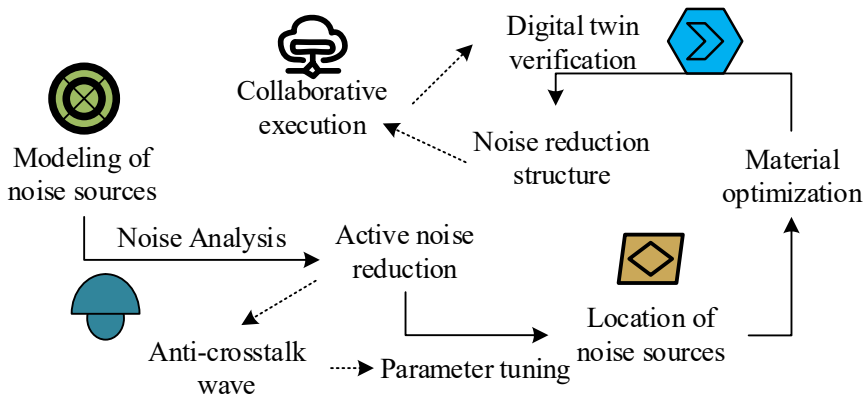

Fig. 3 ISSA-based noise reduction strategy for power system energy storage converters (Source from: author self-drawn)

In Fig. 3, during noise source modeling and localization, kernel principal component analysis is used to reduce the dimension of noise spectral features. Then, the dominant noise components are extracted to construct a noise feature vector, which serves as the input for ISSA optimization. In the ISSA-driven active noise control loop, the generation of inverse sound waves is adaptive, where the switching frequency and cooling fan speed of the converter constitute the state space, and the amplitude of the inverse sound wave is defined as the action space. The output of the controller is calculated using Equation (5).

$$u(t') = K_p e(t') + K_{i'} \int_0^{t'} e(\tau) d\tau \tag{5}$$

In Equation (5), where $e(t')$ denotes the error signal. K_p and $K_{i'}$ are the proportional and integral gains, respectively. $\int_0^{t'} e(\tau) d\tau$ is the time integral of the error. The multi-objective optimization function is calculated using Equation (6).

$$\min\left\{N_{dB}, \frac{\Delta p}{p_{rated}}\right\} \quad \text{s.t.} \quad Z_v \in [Z_{\min}, Z_{\max}] \tag{6}$$

In Equation (6), where N_{dB} is the noise sound pressure level. Δp and p_{rated} represent the power fluctuation and rated power of the converter, respectively. Z_v defines the range of the virtual impedance constraint. $Z_{\min}$ and $Z_{\max}$ represent the minimum virtual impedance and maximum virtual impedance, respectively. Furthermore, ISSA dynamically adjusts the learning rate and exploration noise variance of the deep deterministic policy gradient to improve noise reduction stability and policy convergence speed. In the system-level coordinated noise reduction architecture, the cloud and edge sides are responsible for generating global optimization parameters and adjusting local control parameters in real time, respectively.

2.2 MOPSO-ISSA-based noise reduction and control optimization model

Although the noise reduction strategy for power system energy storage converters based on ISSA efficiently searches for the optimal solution in a complex high-dimensional parameter space, ISSA, as a single-objective optimization algorithm, fails to optimize multiple conflicting objectives such as noise reduction, energy efficiency, and cost at the same time. In addition, the control of converters requires the integration of multiple variables including controller gains and filter parameters. ISSA cannot adjust the noise reduction parameters in real time under complex operating conditions [18]. MOPSO generates a set of trade-off solutions and allows designers to select the best one based on their needs. It also maintains optimization performance under disturbance scenarios such as load fluctuations. Therefore, this study applies MOPSO to optimize ISSA. The operating mechanism of this algorithm is shown in Fig. 4.

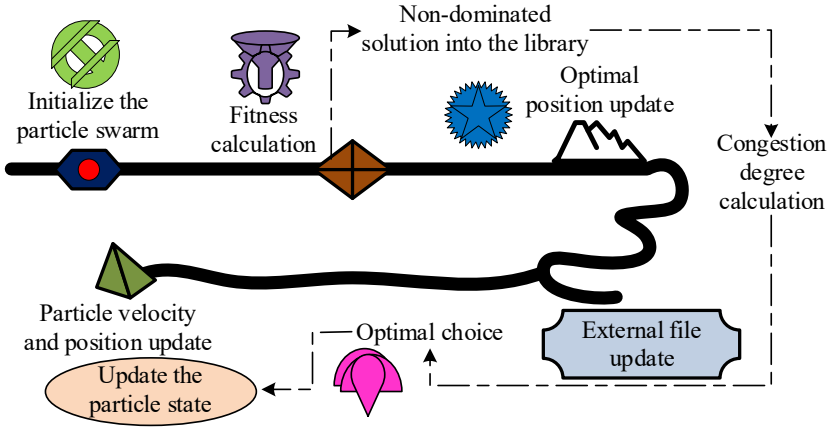

Fig. 4 Operating mechanism of MOPSO (Source from: author self-drawn)

In Fig. 4, MOPSO performs multi-objective optimization by searching for the

Pareto optimal solution set and evaluates solutions using Pareto dominance. The external archive management adopts an adaptive grid method to divide the objective space and retains solutions in sparse regions preferentially by calculating crowding distance, ensuring the even distribution of the solution set. The calculation of crowding distance is shown in Equation (7) [19].

$$CD(O)=\sum_{m=1}^{M}\frac{\left|f_m(O+1)-f_m(i-1)\right|}{f_m^{\max}-f_m^{\min}} \tag{7}$$

In Equation (7), where $f_m^{\max}$ and $f_m^{\min}$ denote the maximum and minimum values of the m-th objective function, respectively. M is the number of objective functions. $f_m(O+1)$ represents the objective function value of the next individual adjacent to individual O under the m-th objective function. $f_m(i-1)$ is the objective function value of the previous individual adjacent to individual O under the m-th objective function. The computation of the Pareto optimal solution set is shown in Equation (8).

$$P^*=\left\{x\in\Omega\middle|\nexists Y\in\Omega:Y\prec x\right\} \tag{8}$$

In Equation (8), where Ω denotes the feasible solution space, x and Y respectively represent a candidate solution in the optimization problem and a candidate solution in the feasible solution space. During the dynamic parameter adjustment, the inertia weight decreases with the number of iterations. The global optimal solution is selected using the roulette wheel method, where particles in sparse grid regions have a higher probability of being chosen. The elitist preservation strategy then removes individuals dominated by new solutions. The main improvements of ISSA through MOPSO include multi-objective collaborative optimization, diversity maintenance, and an online rolling mechanism, as illustrated in Fig. 5.

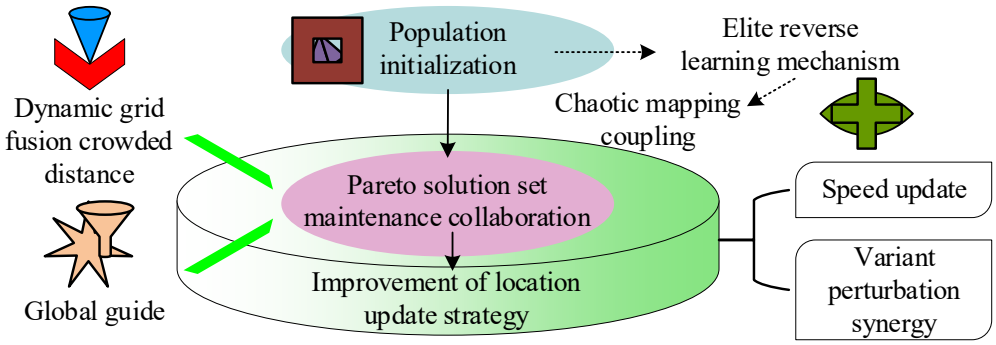

Fig. 5 Optimization process of ISSA by MOPSO (Source from: author self-drawn)

As shown in Fig. 5, for population initialization, MOPSO introduces the chaotic mapping mechanism from ISSA to generate the initial particle swarm, and then creates reverse particles based on elite solutions from ISSA to expand the search range. MOPSO and ISSA divide the objective space and filter non-dominated solutions, jointly optimizing the uniformity of the external archive

distribution. The improved position updating strategy combines velocity update and mutation perturbation. The fuzzy inference system from ISSA dynamically adjusts the weights in the velocity update process. The calculation of the linearly decreasing inertia weight is shown in Equation (9).

$$W(t) = W_{\max} - \frac{(W_{\max} - W_{\min}) \cdot t}{T} \tag{9}$$

In Equation (9), where $W(t)$ denotes the inertia weight in the t-th iteration. $W_{\max}$ and $W_{\min}$ represent the initial and final inertia weights, and T is the total number of iterations. The expression of ISSA disturbance archive is shown in Equation (10) [20].

$$X_{rep}^{new} = X_{rep} + \gamma \cdot randn(D) \tag{10}$$

In Equation (10), where γ represents the dimension-related disturbance amplitude, and D indicates the solution dimension, X_{rep} represents the original individual state before performing the perturbation operation. The mutation perturbation mechanism includes Gaussian mutation from MOPSO and differential mutation from ISSA. Their combined effect reduces the risk of falling into local optima. Based on this, the study designs a noise reduction and control optimization model for energy storage converters using MOPSO-ISSA, as shown in Fig. 6.

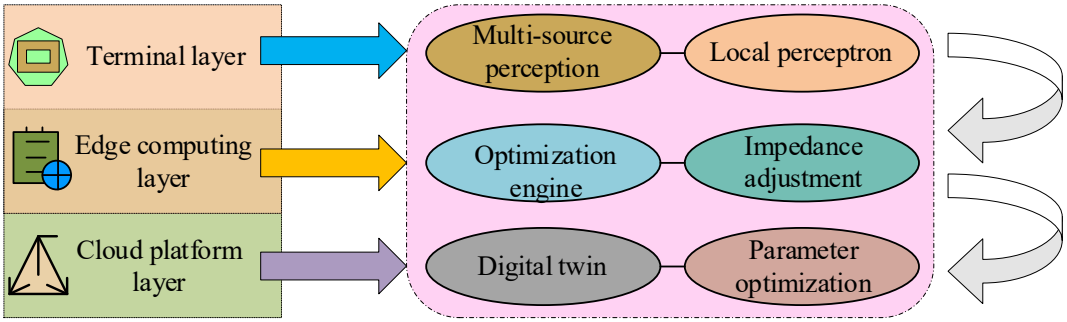

Fig. 6 Noise reduction and control optimization model for energy storage converters based on MOPSO-ISSA (Source from: author self-drawn)

In Fig. 6, the MOPSO-ISSA model structure includes the terminal layer, edge computing layer, and cloud platform layer. The terminal layer deploys vibration sensors and current harmonic detection units to collect real-time data such as temperature rise and switching noise. The edge computing layer uses the ISSA-based real-time optimization engine, where the input data are noise spectrum characteristics and load fluctuation rate, and the output data are switching frequency and anti-phase sound wave phase. The calculation of the reverse learning strategy is shown in Equation (11).

$$X_{opposite} = UB + LB - X_{best} \tag{11}$$

In Equation (11), where UB and LB represent the upper and lower bounds of the search space, X_{best} is the current optimal solution. The calculation of the harmonic distortion noise index is shown in Equation (12).

$$THD_N = \sqrt{\frac{\sum_{h=2}^{H}(U_h / U_1)^2}{SNR}} \times 100\% \tag{12}$$

In Equation (12), where U_h and U_1 denote the voltage amplitude of the h-th harmonic and the fundamental frequency, respectively, and SNR is the signal-to-noise ratio. The calculation of the insertion loss of the sound insulation device is shown in Equation (13).

$$IL = 10\log_{10}(\frac{W_{without}}{W_{with}}) \tag{13}$$

In Equation (13), where $W_{without}$ and W_{with} represent the sound power before and after applying the insulation device, respectively. The adjustment of adaptive virtual impedance is based on the MOPSO multi-objective solution set and dynamically balances noise suppression and system stability. The cloud platform layer includes digital twins and global parameter optimization. It solves the Pareto front using MOPSO and finally generates a control parameter library that is pushed to the edge layer.

3. Performance of the MOPSO-ISSA-based noise reduction and control model for converters

3.1 Performance comparison of the converter noise reduction and control model

To verify the performance of the proposed noise reduction and control model for power converters, this study compared it with the following models: Optimal Order Adaptation and Improved Sparrow Search Algorithm (OOA-ISSA), Dung Beetle Optimizer and Variational Mode Decomposition (DBO-VMD), and Continuous Wavelet Transform and Least Mean Square (CWT-LMS). A 1250 kW centralized energy storage converter was selected for testing. Its topology was T-type three-level and the cooling method was air cooling. In the grid simulation system, the AC port voltage was set to 35 kV, and the load fluctuated from 20% to 120% of the rated power. A wideband sound pressure meter (20 Hz–20 kHz) was used as the sensor, placed 1 m in front of the converter and 0.5 m on the side. The population size and iteration number for both MOPSO-ISSA and OOA-ISSA were set to 50 and 200, respectively. The inertia weight of MOPSO-ISSA was 0.6, and the learning factor was 1.8. The search step size of OOA-ISSA was set to 0.1. For DBO-VMD, the number of modes and penalty factor were set to 8 and 2000, respectively. The filter order of CWT-LMS was set to 32. The experimental datasets

included the CIGRE B4 DC Grid Test System dataset and the IEEE PES converter noise database, which were used as the training and testing sets. The CIGRE dataset contained current and voltage waveforms and noise spectra under typical operating conditions of energy storage converters. The IEEE PES dataset included noise characteristics of converters with different topologies and contained abundant information on power quality disturbances. The study first tested the loss values of the four models in the training and testing sets. The results are shown in Fig. 7.

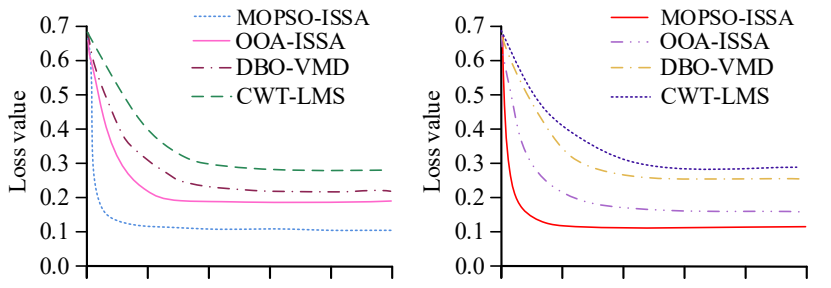

Fig. 7 Comparison of loss values in training and testing sets (Source from: author self-drawn)

According to Fig. 7, the proposed model showed the fastest convergence in both the training and testing sets. It reached convergence at around 50 iterations, and the loss value remained stable at approximately 0.1. In contrast, the other three comparison models converged more slowly. Their loss values were higher than that of MOPSO-ISSA in both datasets. CWT-LMS, in particular, only reached convergence after nearly 200 iterations in the testing set. These results demonstrated that MOPSO-ISSA had excellent convergence performance and performed better in both loss reduction and stability, showing stronger adaptability. The study then tested the amplitude of the generated data by the four models in the training and testing sets. Model performance was further analyzed from two aspects: normalized frequency and noise value distribution. The results are shown in Fig. 8.

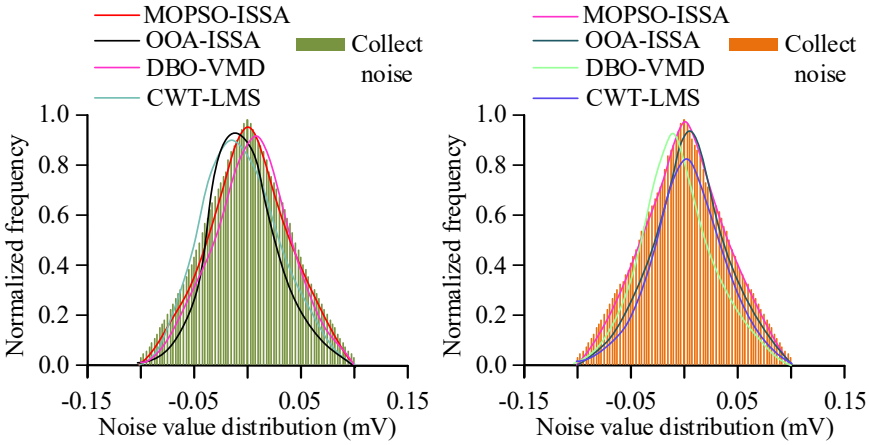

Fig. 8 Comparison of generated data amplitudes in training and testing sets (Source from: author self-drawn)

In Fig. 8(a), the amplitude distribution of the noise generated by the proposed model was the closest to that of the actual collected noise. Although the curves of the comparison models overlapped with the real noise in most regions, there were notable differences in normalized frequency within the -0.05~0.05 mV interval, indicating lower simulation accuracy. In Fig. 8(b), the generated data of the proposed model still matched the actual noise distribution closely. Its peak and curve shape showed the best alignment among the four models. The comparison models showed deviations in normalized frequency near the peak values, especially CWT-LMS, which had the most obvious deviation around -0.15 mV and 0.15 mV. These results indicated that the proposed model had good generalization ability and achieved better fitting of collected noise. Finally, the study analyzed the noise suppression effects of the four models in the training and testing sets, as shown in Fig. 9.

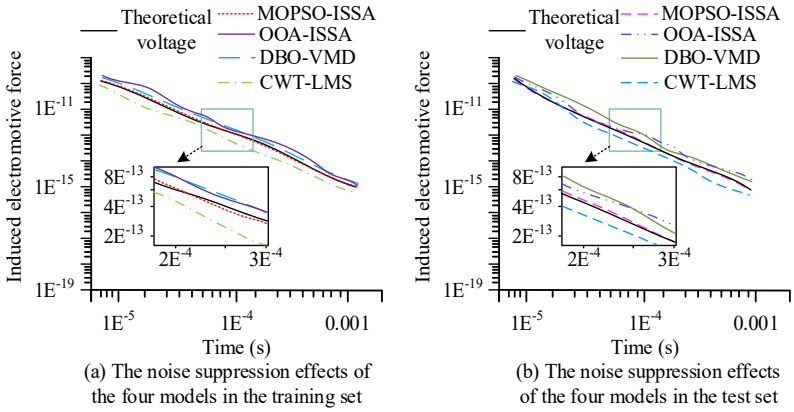

Fig. 9 Comparison of noise suppression effects in training and testing sets (Source from: author self-drawn)

In Fig. 9(a), the MOPSO-ISSA curve remained highly consistent with the theoretical voltage curve. Especially in the local zoomed-in region from $2E^{-4}$ to $3E^{-4}$ s, the trend of induced electromotive force almost completely matched the theoretical voltage. The other three models followed the theoretical curve overall, but showed more noise residues, and their curves deviated more from the reference compared to the proposed model. In Fig. 9(b), the proposed model continued to perform well, showing the best fit to the theoretical voltage curve among the four models. The comparison models showed greater deviations from the theoretical voltage, and their noise suppression effects fluctuated over time. These results demonstrated that the proposed model had better noise suppression performance and generalization ability.

3.2 Analysis of the practical application of the converter noise reduction and control model

To further evaluate the practical performance of the proposed noise reduction control model for converters, this study tested the model using real operational data from the 2024 Kashgar Source-Grid-Load-Storage Integration Project. An A-weighted sound level meter was placed 1 meter in front of and 0.5 m to the side of the converter. Voltage waveforms were synchronously recorded through the existing SCADA system. The grid voltage was maintained at the actual 35 kV, and the load fluctuation range was set from 30% to 110% of the rated power. The study first analyzed the noise reduction results of the four models, as shown in Fig. 10.

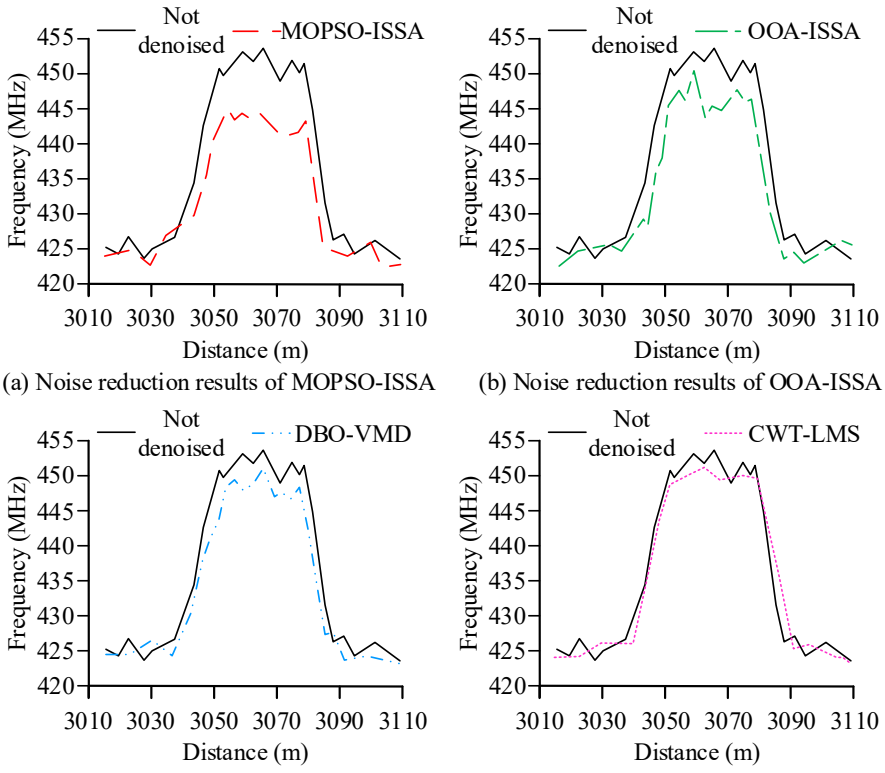

(a) Noise reduction results of MOPSO-ISSA (b) Noise reduction results of OOA-ISSA

(c) The noise reduction result of DBO-VMD (d) Noise reduction results of CWT-LMS

Fig. 10 Comparison of noise reduction results (Source from: author self-drawn)

According to Fig. 10, the curve without noise reduction showed noticeable fluctuations and significant noise interference. After denoising with the MOPSO-ISSA model, the curve became smoother and successfully preserved signal features in the peak region between 3050 and 3070 m. Although the denoised curve of the OOA-ISSA model was relatively smooth, it showed clear deviations at the peaks, indicating weak signal restoration. The DBO-VMD model exhibited large fluctuations at both ends of the distance range, and residual noise affected the integrity of the signal. The CWT-LMS model caused obvious distortion after denoising, which could easily result in the loss of peak features. These results showed that the proposed model achieved a better balance between noise removal and signal preservation, demonstrating the best denoising performance among the four. The study then tested the prediction performance of the four models for converter output voltage, as shown in Fig. 11.

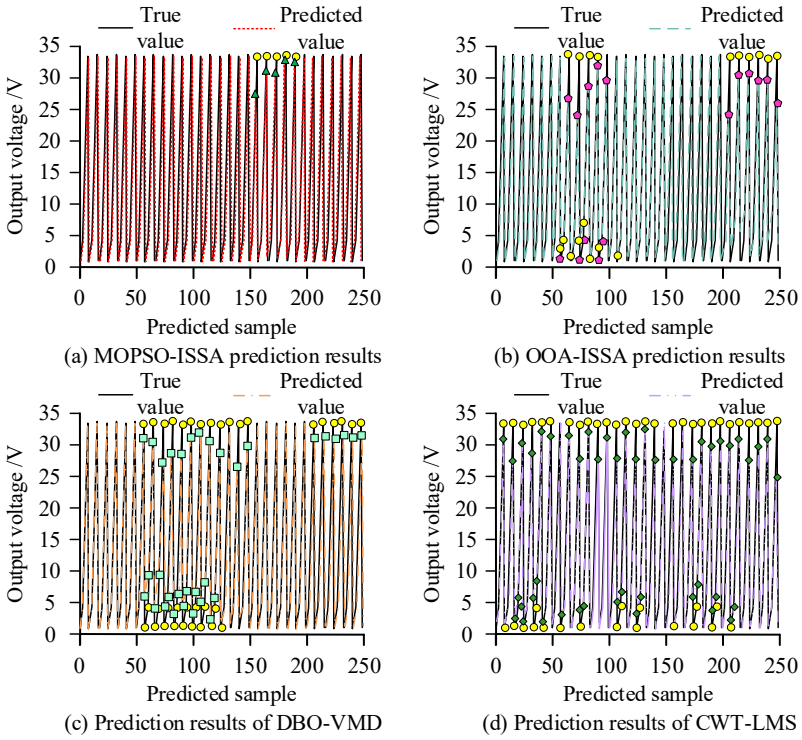

Fig. 11 Comparison of output voltage prediction results (Source from: author self-drawn)

As shown in Fig. 11, the predicted values of the MOPSO-ISSA model closely matched the actual values, with most prediction points tightly aligned with the real voltage curve. Within the sample range of 0 to 250, the model demonstrated excellent prediction accuracy, with only a few points showing minor deviations. In contrast, the other three models showed larger prediction dispersion. In particular, the prediction points of OOA-ISSA and DBO-VMD significantly deviated from the actual values between samples 50 and 150. The CWT-LMS model had the largest deviation from actual values, failing to accurately capture voltage variation patterns. These results indicated that the proposed model achieved the highest accuracy and stability in voltage prediction, providing reliable data support for subsequent noise reduction and control optimization. Finally, the study tested the noise reduction and dynamic performance of the four models, and the results are presented in Table 1.

Table 1

Noise reduction and dynamic performance results of the four models

Index	Model			
	MOPSO-ISSA	OOA-ISSA	DBO-VMD	CWT-LMS
Noise suppression (dB)	75.62±0.15	71.45±0.25	72.15±0.84	69.14±0.41

Total Harmonic Distortion (%)	1.32	2.64	3.25	4.75
Mode switching delay (ms)	45.85	92.45	123.17	187.95
Voltage pulsation (%)	±0.31	±0.74	±1.25	±2.17
Hardware cost/ten thousand yuan	6.31	8.72	9.46	11.46
The algorithm takes time (s)	92.56	136.14	182.14	214.75

As shown in Table 1, the proposed model achieved the most significant noise suppression effect, with a Total Harmonic Distortion (THD) of 1.32%, which was much lower than the other models. The THD values of OOA-ISSA and DBO-VMD were 2.64% and 3.25%, respectively. CWT-LMS showed the highest voltage fluctuation at ±2.17%, while the proposed model maintained a minimal fluctuation of only ±0.31%. Regarding the mode switching delay, the proposed model had the shortest delay of 45.85 ms, whereas OOA-ISSA and DBO-VMD had delays of 92.45 ms and 123.17 ms, respectively. These results confirmed that the proposed model outperformed the others in terms of noise suppression, power quality, and dynamic response, making it more suitable for application in power IoT energy storage converters.

4. Conclusion

Existing noise reduction methods faced challenges in coordinating control stability and denoising performance under dynamic operating conditions. To address this issue, this study put forward a noise reduction and control optimization model for energy storage converters based on MOPSO-ISSA. Vibration sensors and current harmonic detection units were deployed, and real-time data such as temperature rise and switching noise were collected. The experimental results showed that the MOPSO-ISSA curve consistently overlapped with the theoretical voltage curve, especially in the locally enlarged region between 2E-4 and 3E-4 seconds, where the trend of induced electromotive force closely matched the theoretical voltage. Although the other three models generally followed the theoretical voltage curve, they retained more residual noise, and their deviations were more noticeable compared to the proposed model. The predicted values generated by the MOPSO-ISSA model also demonstrated a high degree of alignment with the actual values. Most prediction points closely followed the real

voltage curve, showing excellent prediction accuracy within the 0–250 sample interval, with only minor deviations at a few points. In contrast, the other three models showed larger prediction dispersion. In summary, the proposed model delivered outstanding noise reduction performance and generalization ability, making it more suitable for energy storage converters in power IoT applications. The study pioneered a deep fusion framework that combines MOPSO and ISSA. MOPSO generates a Pareto optimal solution set to handle multi-objective conflicts and combines ISSA's dynamic sine perturbation and Gaussian shift strategy to achieve local parameter refinement. However, the selection of the Pareto solution set in this model relied on static weight coefficients, which made it difficult to adapt to extreme conditions such as sudden grid disturbances. In the future, voiceprint recognition technology will be introduced, and the multi-objective weight coefficients will be automatically adjusted based on the characteristics of the noise spectrum, improving the model's adaptability to aging components.

Funding Statement: This work is supported by the Science and Technology Project of State Grid Fujian Electric Power Co., Ltd. Research and Demonstration Application of Autonomous Collaborative Control and Energy Saving and Noise Reduction Methods for Shared Energy Storage System in Distribution Area, No. 521304230007

REFERENCE

[1] Ma Z, Wang S, Huang Q, Yang Y. A review of radiated EMI research in power electronics systems. IEEE Journal of Emerging and Selected Topics in Power Electronics, 2023, 12(1): 675-694.

[2] Montazerolghaem R, Adib E, Semiromizadeh J, Wheeler P. Zero-voltage-switching high-step-down buck converter with continuous output current. IEEE Transactions on Power Electronics, 2023, 38(10): 12886-12894.

[3] Asvadi-Kermani O, Felegari B, Momeni H, Davari A, Rodriguez J. Dynamic neural-based model predictive voltage controller for an interleaved boost converter with adaptive constraint tuning. IEEE Transactions on Industrial Electronics, 2023, 70(12): 12739-12751.

[4] Ma Z, Wang S, Sheng H, Lakshmikanthan S. Modeling, analysis and mitigation of radiated EMI due to PCB ground impedance in a 65 W high-density active-clamp flyback converter. IEEE Transactions on Industrial Electronics, 2023, 70(12): 12267-12277.

[5] Ahmed A, Li L, Jung M, Li S, Baltimas D, Rebeiz G. 140-GHz 2-D Scalable On-Grid 8×8-Element Transmit–Receive Phased Arrays With Up/Down Converters Demonstrating a 5.2-m Link at 16 Gbps. IEEE Transactions on Microwave Theory and Techniques, 2024, 72(5): 2852-2868.

[6] Gharehchopogh F S, Namazi M, Ebrahimi L, Abdollahzadeh B. Advances in sparrow search algorithm: a comprehensive survey. Archives of Computational Methods in Engineering, 2023, 30(1): 427-455.

[7] Xue J, Shen B. A survey on sparrow search algorithms and their applications. International Journal of Systems Science, 2024, 55(4): 814-832.

[8] Cen J, Zeng L, Liu X, Wang F, Deng S, Yu Z, Zhang G, Wang W. Research on energy-saving optimization method for central air conditioning system based on multi-strategy improved sparrow search algorithm. International Journal of Refrigeration, 2024, 160(8): 263-274.
[9] Zhang W, Geng H, Li C, Gen M, Zhang G, Deng M. Q-learning-based multi-objective particle swarm optimization with local search within factories for energy-efficient distributed flow-shop scheduling problem. Journal of Intelligent Manufacturing, 2025, 36(1): 185-208.
[10] Shu X, Liu Y, Liu J, Yang M, Zhang Q. Multi-objective particle swarm optimization with dynamic population size. Journal of Computational Design and Engineering, 2023, 10(1): 446-467.
[11] Cao Y, Bai Y, Mitrovic V, Fan B, Dong D, Burgos R. A three-level buck–boost converter with planar coupled inductor and common-mode noise suppression. IEEE Transactions on Power Electronics, 2023, 38(9): 10483-10500.
[12] Nabih A, Li Q. Design of 98.8% efficient 400-to-48-V $ LLC $ converter with optimized matrix transformer and matrix inductor. IEEE Transactions on Power Electronics, 2023, 38(6): 7207-7225.
[13] Babayomi O, Zhang Z, Li Z, Heldwein M L, Rodriguez J. Robust predictive control of grid-connected converters: Sensor noise suppression with parallel-cascade extended state observer. IEEE Transactions on Industrial Electronics, 2023, 71(4): 3728-3740.
[14] Vaithianathan M. Digital Signal Processing for Noise Suppression in Voice Signals. International Journal of Advanced Research and Interdisciplinary Scientific Endeavours, 2024, 4(1): 198-208.
[15] Yu Z, Liang Y, Lan H, Chen L, Song J, Song S. A time-domain reconfigurable second-order noise shaping ADC with single fan-out gated delay cells. IEEE Transactions on Very Large Scale Integration (VLSI) Systems, 2023, 31(6): 902-905.
[16] Ariyanto S R, Suprayitno S, Wulandari R. Design of metallic catalytic converter using pareto optimization to improve engine performance and exhaust emissions. Automotive Experiences, 2023, 6(1): 200-2015.
[17] Issaadi W, Issaadi S. Influence of the sampling frequency on various maximum power point tracking commands[J]. Revue Roumaine des sciences techniques—Série électrotechnique et énergétique, 2023, 68(1): 12-17.
[18] Serban E, Pondiche C, Ordonez M. Analysis and design of bidirectional parallel-series DAB-based converter. IEEE Transactions on Power Electronics, 2023, 38(8): 10370-10382.
[19] Shahgholian G, Zanjani S M A. A study of voltage sag in distribution system and evaluation of the effect of wind farm equipped with doubly-fed induction generator[J]. Revue Roumaine des sciences techniques—Série électrotechnique et énergétique, 2023, 68(3): 271-276.
[20] Jia N, Tian X, Xue L, Bai H, Tolbert L, Cui H. Integrated common-mode filter for GaN power module with improved high-frequency EMI performance. IEEE Transactions on Power Electronics, 2023, 38(6): 6897-6901.